A Switching High-Gain Observer Approach for Estimating the State of Charge of Metal Hydride Storage Tanks

Mingrui Chen, Andreu Cecilia, *Member, IEEE*, Jing Na, *Member, IEEE*, Carles Batlle and Ramon Costa-Castelló, *Senior Member, IEEE*,

***Abstract*—State of charge serves as a critical metric for the monitoring and operation of metal hydride storage systems. As the state of charge cannot be obtained through direct measurement, it is typically inferred by constructing state observers that reconstruct the internal states of the storage system. However, the system exhibits an equilibrium region between absorption and release, in which it becomes non-observable. In comparison to previous works, we consider a model that includes thermal effects, which reduces the unobservable region. To deal with the piecewise smooth nature of the model, this paper proposes a novel nonlinear switching high-gain observer for metal hydride storage tank systems. The observability properties of a third-order state-space representation of the system are systematically investigated and sufficient conditions ensuring observer convergence are established under the assumption of synchronous switching between the observer and the system. Furthermore, the robustness of the proposed observer is examined in scenarios where asynchronous switching occurs between the observer and the system. Finally, the effectiveness of the proposed method is verified by both numerical simulations and experimental studies.**

***Index Terms*—Metal hydride storage tank, State of charge (SOC), High-gain observer, Switched system**

I. Introduction

This work was partially supported by the Ministerio de Ciencia, Innovación y Universidades, la Agencia y del Fondo Europeo de Desarrollo Regional (Project DECODER (PID2024-158394OB-C22) funded by MICIU/AEI/10.13039/501100011033/FEDER UE)", as part of the AVANTE project, supported by the Spanish Ministry of Science, Innovation and Universities and the National Research Agency (PDC2025-165204-C22, financed by MICIU/AEI/10.13039/501100011033) and Supported by the 'Siemens Energy AI Chair: Energy Sustainability for a Decarbonized Society 5.0' (TSI-100930-2023-5), funded by the Secretary of State for Digitalization and Artificial Intelligence through the ENIA 2022 Chairs call, and co-funded by the European Union-Next Generation EU. This work also receives partial support from the National Natural Science Foundation of China under grants (62433012, 62461160260, 62273169), as well as funding from the China Scholarship Council (CSC) under Grant (202208530009).

Mingrui Chen is affiliated with the Institut de Robòtica i Informàtica Industrial, CSIC-UPC. C/ Llorens i Artigas 4-6, 08028 Barcelona, Spain. (*mail: chenmingrui2018@gmail.com*)

Andreu Cecilia and Ramon Costa-Castelló are affiliated with the Universitat Politècnica de Catalunya, Avinguda Diagonal, 647, 08028 Barcelona, Spain. (*mail: andreu.cecilia@upc.edu, ramon.costa@upc.edu*)

Jing Na is affiliated with the Faculty of Mechanical and Electrical Engineering, Kunming University of Science and Technology, and is also associated with the Yunnan Key Laboratory of Intelligent Control and Application, Kunming, 650500, P.R. China. (*mail: najing25@163.com*)

Carles Batlle is affiliated with the Departament de Matemàtiques, Institut d'Organització i Control, EPSEVG, UPC, 08800 Vilanova i la Geltru, Spain. (*mail: carles.batlle@upc.edu*)

METAL hydride (MH) storage tanks are widely regarded as a promising technology for solid-state hydrogen storage due to their high volumetric energy density and inherent safety advantages [1]. In practical applications such as renewable energy systems, hybrid power systems, and hydrogen-based backup power units, the reliable operation of MH tanks requires accurate knowledge of their internal storage condition [2]. Among the relevant indicators, the state of charge (SOC), which represents the proportion of the current hydrogen content relative to the maximum storage capacity, plays an important role in monitoring, control, and safety management [3]. Despite its importance, the SOC of a MH storage tank is not directly measurable with existing sensing technologies. Consequently, it has to be inferred from measurable variables, including temperature, pressure, and hydrogen flow rate. Model-based state observers [4], [5] provide a systematic framework to address this issue by reconstructing the internal state of the tank using its dynamic model and measured signals. Nevertheless, SOC estimation remains a challenging task, mainly due to the nonlinear behavior of the physicochemical processes and the hybrid nature of hydrogen absorption and desorption dynamics.

A primary difficulty in SOC estimation is the existence of an equilibrium region between absorption and desorption. In this region, the system exhibits intrinsic non-observability, as identical pressure measurements may correspond to different internal hydrogen content. As a result, even with perfect measurements, the internal state cannot be uniquely reconstructed. Existing observer design methods mostly rely on simplified low-order state-space models to reduce computational complexity [6], [7]. Although these models can estimate the SOC with reasonable accuracy, the primary issue lies in the existence of large unobservable regions, namely equilibrium regions. When the system traverses these regions, the observer loses its estimation capability, which significantly reduces the convergence rate of the observer and robustness. This limitation prompts us to consider models that minimise non-observable regions and to design new observers based on these models.

In this work, a nonlinear switching high-gain observer is proposed for SOC estimation in MH storage tanks. More specifically, the main contributions of this work are summarized as follows.

1) The proposed approach relies on a third-order state-space representation of the MH tank, for which a comprehen-

NOMENCLATURE

Abbreviations

SOC	State of charge
MH	Metal hydride
USDE	Unknown system dynamic estimator

Parameters

V_{MH}	Volume of the MH (m^3)
f_{in}	Normalized mass-flow rate of hydrogen ($kg/m^3/s$)
C_d	Desorption constant ($1/s$)
V_g	Normalized volume of hydrogen
f_r	Normalized sorption mass-flow rate of hydrogen ($kg/m^3/s$)
ε	Porosity of the MH
C_a	Absorption constant ($1/s$)
F_{in}	Flow rate of hydrogen (Ln/min)
V_{H_2}	Maximum volume of hydrogen that can be absorbed (m^3)
P	Pressure of hydrogen (Pa)
k_p	Proportional coefficient
ρ_g	Density of hydrogen (kg/m^3)
P_0	Atmospheric pressure ($101\,325$ Pa)
M_{H_2}	Molar mass of hydrogen (2.016×10^{-3} kg/mol)
R	Universal gas constant ($8.314\,J/mol/K$)
ρ_s	Density of the MH (kg/m^3)
ρ_{H_2}	Density of hydrogen in standard state (kg/m^3)
V_s	Normalized volume of the MH
P_{pipe}	Pipe pressure (Pa)
φ, φ_0	Plateau flatness coefficients
β	Plateau hysteresis coefficient
ρ_{s0}	Empty density of the MH without any hydrogen (kg/m^3)
$P_{eq,d}$	Equilibrium pressure of desorption (Pa)
ρ_{ss}	Saturated density of the MH with complete absorption of hydrogen (kg/m^3)
$P_{eq,a}$	Equilibrium pressure of absorption (Pa)
m_{total}	Maximum hydrogen capacity (kg)
ΔS_d	Entropy change for desorption ($J/mol/K$)
E_d	Activation energy of desorption (J/mol)
ΔH_d	Enthalpy change for desorption (J/mol)
E_a	Activation energy of absorption (J/mol)

Subscripts

a	Absorption
σ	Switching signal
d	Desorption

sive observability analysis is performed.

2) Based on the observability analysis, a switching high-gain observer is constructed to reconstruct the internal states of the MH tank. Sufficient conditions are established to guarantee convergence of the observer under the assumption of synchronous switching between the observer and the plant.
3) The robustness of the proposed approach is investigated in scenarios where the mode of operation of the observer and the plant are temporarily de-synchronized, which naturally arise in practical implementations.
4) The effectiveness of the proposed SOC estimation framework is demonstrated through a numerical simulation and experimental validation on an MH storage tank setup.

Section II describes the mathematical modeling of the MH storage tank and formulates the observer design and SOC estimation tasks. Then, Section III examines the system observability. The observer design methodology is detailed in Section IV. Numerical simulation results are reported in Section V, followed by experimental verification using an MH tank setup in Section VI.

II. PROBLEM FORMULATION

A. Mathematical Model of MH tanks

This work adopts an established mathematical description of the MH storage tank reported in [8]. The system dynamics are expressed in a state-space representation as follows.

$$\dot{\mathbf{x}} = \begin{bmatrix} \dfrac{u_1 - f_r}{V_g} \\ \dfrac{f_r}{V_s} \\ \dfrac{f_r \dfrac{\Delta H}{M_{H_2}} + f_r x_3 (C_{pg} - C_{ps}) + Q}{V_g C_{pg} x_1 + V_s C_{ps} x_2} \end{bmatrix}, \tag{1a}$$

$$\mathbf{y} = \begin{bmatrix} \dfrac{x_1 x_3 R}{M_{H_2}} \\ x_3 \end{bmatrix}. \tag{1b}$$

The state vector is defined as: $\mathbf{x} = [x_1, x_2, x_3]^\top = [\rho_g, \rho_s, T]^\top$, where ρ_g [kg/m^3] and ρ_s [kg/m^3] denote the hydrogen density and the metal hydride density, respectively, and T [K] represents the tank temperature. Both densities evolve according to the hydrogen absorption and desorption processes. The system is driven by measurable inputs, $\mathbf{u} = [u_1, u_2]^\top = [f_{in}, T_{amb}]^\top$, where f_{in} [$kg/m^3/s$] is the normalized hydrogen mass-flow rate and T_{amb} [K] is the ambient temperature. The measurable outputs are given by $\mathbf{y} = [y_1, y_2]^\top = [P, T]^\top$, with P [Pa] denoting the tank pressure.

In practice, physical limitations impose boundedness on the system variables, such that the state, input, and output vectors evolve within compact sets.

The quantities V_g and V_s represent the normalized volumes of hydrogen and metal hydride, respectively. The parameters C_{pg} and C_{ps} correspond to their specific heat capacities. The term ΔH [J/mol] denotes the enthalpy variation associated with the reaction (absorption: ΔH_a, desorption: ΔH_d), and the heat transfer term Q [W/m^3] is modeled as:

$$Q = \frac{k_{amb}(T_{amb} - T)}{V_{MH}}, \tag{2}$$

where k_{amb} is the heat transfer coefficient. Additional constants include the universal gas constant R [$8.314\,J/mol/K$] and the molar mass of hydrogen M_{H_2} [2.016×10^{-3} kg/mol].

The normalized hydrogen sorption rate f_r is described by a piecewise nonlinear function, accounting for both absorption and desorption regimes depending on the pressure conditions.

$$\begin{cases} f_{r,a} = C_a e^{-\frac{E_a}{RT}} \ln\left(\frac{P}{P_{eq,a}}\right)(\rho_{ss} - \rho_s), & P > P_{eq,a}, \\ f_{r,d} = C_d e^{-\frac{E_d}{RT}} \left(\frac{P - P_{eq,d}}{P_{eq,d}}\right)\rho_s, & P < P_{eq,d}, \\ f_{r,e} = 0, & \text{otherwise.} \end{cases} \tag{3}$$

where C_a [$1/s$] and C_d [$1/s$] denote the rate coefficients for absorption and desorption, respectively. The parameters E_a [J/mol] and E_d [J/mol] represent the corresponding activation energies. $P_{eq,a}$ [Pa] and $P_{eq,d}$ [Pa] denote the

equilibrium pressures linked to absorption and desorption.The notation ρ_{ss} [$\mathrm{kg/m^3}$] refers to the density of the metal hydride when fully saturated with hydrogen, whereas ρ_{s0} [$\mathrm{kg/m^3}$] represents the density of the alloy in the absence of hydrogen.

The equilibrium pressures $P_{eq,a}$ and $P_{eq,d}$ that define the boundaries for the function switching in (3) are computed as

$$P_{eq,a} = P_0 \cdot e^{\left(\frac{\Delta S_d}{R} - \frac{\Delta H_d}{R \cdot T} + (\varphi+\varphi_0)\tan\left[\pi\left(\frac{\rho_s-\rho_{s0}}{\rho_{ss}-\rho_{s0}}-0.5\right)\right]+\frac{\beta}{2}\right)}, \quad (4)$$

$$P_{eq,d} = P_0 \cdot e^{\left(\frac{\Delta S_d}{R} - \frac{\Delta H_d}{R \cdot T} + (\varphi-\varphi_0)\tan\left[\pi\left(\frac{\rho_s-\rho_{s0}}{\rho_{ss}-\rho_{s0}}-0.5\right)\right]-\frac{\beta}{2}\right)}, \quad (5)$$

where P_0 [Pa] denotes the atmospheric pressure. The parameters φ [-] and φ_0 [-] represent the flatness of the plateau area, whereas β [-] defines the hysteresis impact of the plateau. ΔH_d [$\mathrm{J/mol}$] and ΔS_d [$\mathrm{J/mol/K}$] refer to the changes in enthalpy and entropy linked to the desorption process, respectively.

Finally, the saturated density ρ_{ss} is expressed as

$$\rho_{ss} = \rho_{s0} + \frac{V_{H_2} \cdot \rho_{H_2}}{V_{MH} \cdot (1-\varepsilon)} \quad (6)$$

where V_{H_2} [$\mathrm{m^3}$] denotes the hydrogen storage capacity of the tank, and ρ_{H_2} [$\mathrm{kg/m^3}$] represents the density of hydrogen under standard conditions ($1\,\mathrm{atm}$, $0\,^\circ\mathrm{C}$). V_{MH} [$\mathrm{m^3}$] corresponds to the metal hydride volume, and ε denotes its porosity. For simplicity, ε is assumed to remain constant during both the charging and discharging processes [3], [8].

B. Main objective

The primary goal of this study is to assess the SOC of the MH tank described by model (1) using the measured signals $\mathbf{y}, \mathbf{u}$ in real time. In particular, we will solve this problem by means of a nonlinear observer that uses the temperature, pressure and flow rate as measured signals to estimate the state $\mathbf{x}$. Subsequently, the SOC of the MH tank can be derived from the estimated state. More precisely, the SOC of the MH tank is calculated using the following expression [7]:

$$soc_{tank} = \frac{V_{MH} \cdot V_g}{m_{total}} x_1 + \frac{V_{MH} \cdot V_s}{m_{total}} (x_2 - \rho_{s0}), \quad (7)$$

where m_{total} represents the maximum hydrogen capacity of the MH tank. Since the variables x_1 and x_2 in the definition are unknown (all the remaining ones are constants and assumed known) the SOC estimation becomes a problem of estimating the states x_1 and x_2 in real-time. Thus, we convert the problem of estimating the SOC of MH tanks into an observer design problem.

More specifically, the observer design problem can be formulated as the construction of a dynamical system of the form

$$\dot{\hat{\mathbf{x}}} = \mathbf{j}(\hat{\mathbf{x}}, \mathbf{y}, \mathbf{u}), \quad (8)$$

with state $\hat{\mathbf{x}} \in \mathcal{X}$ and vector field $\mathbf{j} : \mathcal{X} \times \mathcal{Y} \times \mathcal{U} \to \mathbb{R}^3$, such that for all initial conditions $\mathbf{x}(0) \in \mathcal{X}$, $\hat{\mathbf{x}}(0) \in \mathcal{X}$,

$$\lim_{t\to\infty} \|\mathbf{x}(t) - \hat{\mathbf{x}}(t)\| = 0. \quad (9)$$

Then, the estimation of SOC, $\hat{soc}_{tank}$, is

$$\hat{soc}_{tank} = \frac{V_{MH} \cdot V_g}{m_{total}} \hat{x}_1 + \frac{V_{MH} \cdot V_s}{m_{total}} (\hat{x}_2 - \rho_{s0}). \quad (10)$$

Prior to revealing the primary outcome of this paper, specifically the observer (8), the observability of the system (1a)-(1b) must be analysed, which shows if the state variable $\mathbf{x}$ can be deduced from the observed variables and the model. This issue is tackled in the next section.

III. Observability properties of the model

Consider the following input-affine nonlinear system:

$$\begin{aligned} \dot{\mathbf{x}} &= \mathbf{f}(\mathbf{x}) + \mathbf{g}(\mathbf{x})\,\mathbf{u} \\ \mathbf{y} &= \mathbf{h}(\mathbf{x}), \end{aligned} \quad (11)$$

where $\mathbf{x} \in \mathbb{R}^n$, $\mathbf{u} \in \mathbb{R}^m$, and $\mathbf{y} \in \mathbb{R}^p$ denote the state, input, and output, respectively.

Based on the definition of instantaneous observability [4], [9], a system is instantaneously observable if distinct state trajectories $\mathbf{x}(t)$ always produce different output trajectories $\mathbf{Y}(\mathbf{x}_a, \mathbf{u}, t)$, which separate after an arbitrarily short time interval [9], [10]. In the context of this work, instantaneous observability, as considered in our case, requires that any three distinct state combinations (ρ_g, ρ_s, T) produce distinguishable pressure and temperature trajectories, P and T, for the tank.

Instantaneous observability can be checked via the rank of the Jacobian matrix of the observability map [11]:

$$O_k(\mathbf{x}, \mathbf{u}, \ldots, \mathbf{u}^{(k-2)}) = \begin{bmatrix} \mathbf{y} \\ \dot{\mathbf{y}} \\ \\ \vdots \\ \mathbf{y}^{(k-1)} \end{bmatrix}. \quad (12)$$

where $\mathbf{u}^k \triangleq \frac{d^k\mathbf{u}}{dt^k}$, $\mathbf{y}^k \triangleq \frac{d^k\mathbf{y}}{dt^k}$, with $k \in \mathbb{N}$. In addition, k should be larger than the order of the state-space system, n, that is, $k \geq n$. If, $\forall x \in \mathbb{R}^n$ and $\forall \mathbf{u}, \ldots, \mathbf{u}^{(k-2)} \in \mathbb{R}^m$,

$$rank\left(\frac{\partial O_k(\mathbf{x}, \mathbf{u}, \ldots, \mathbf{u}^{(k-2)})}{\partial \mathbf{x}}\right) = n, \quad (13)$$

then, the system satisfies the instantaneous observable condition in $(\mathbf{x}, \mathbf{u}, \ldots, \mathbf{u}^{(k-2)})$.

For system (1a)-(1b), the observability map (12) with $k = 3$ is given by:

$$O_3(\mathbf{x}, \mathbf{u}, \dot{\mathbf{u}}) = [y_1, y_2, \dot{y}_1, \dot{y}_2, \ddot{y}_1, \ddot{y}_2]^{\mathrm{T}}. \quad (14)$$

As indicated in (3), f_r is a nonlinear function defined in a piecewise manner. Consequently, the examination of the rank of the Jacobian matrix $J \triangleq \frac{\partial O_3}{\partial \mathbf{x}}$ is categorized into two scenarios:

1) Case 1: $f_r = 0$.
   In this case, the system dynamics simplify to

$$\dot{\mathbf{x}} = \mathbf{f}(\mathbf{x}, \mathbf{u}) = \begin{bmatrix} \frac{u_1}{V_g} \\ 0 \\ \\ \frac{k_{amb} \cdot (u_2 - x_3)}{V_{MH} \cdot (V_g C_{pg} x_1 + V_s C_{ps} x_2)} \end{bmatrix}. \quad (15)$$

The matrix J has the following form:

$$J_{f_r=0} = \begin{bmatrix} \frac{x_3 R}{M_{H_2}} & * & * \\ * & * & 1 \\ * & *_3 & * \\ * & *_4 & * \\ * & *_5 & * \\ * & *_6 & * \end{bmatrix}, \tag{16}$$

where

$$*_3 = -\frac{x_1 R k_{amb}(u_2 - x_3) C_{ps} V_s}{M_{H_2} V_{MH} (V_g C_{pg} x_1 + V_s C_{ps} x_2)^2},$$

$$*_4 = -\frac{k_{amb}(u_2 - x_3) C_{ps} V_s}{V_{MH} (V_g C_{pg} x_1 + V_s C_{ps} x_2)^2},$$

$$*_5 = \frac{u_1}{V_g}\Bigg[-\frac{R k_{amb}(u_2 - x_3) C_{ps} V_s}{M_{H_2} V_{MH} \left(V_g C_{pg} x_1 + V_s C_{ps} x_2\right)^2} + \frac{2 x_1 R k_{amb}(u_2 - x_3) C_{pg} V_g C_{ps} V_s}{M_{H_2} V_{MH} \left(V_g C_{pg} x_1 + V_s C_{ps} x_2\right)^3}\Bigg] + \frac{x_1 R k_{amb}^2 (u_2 - x_3) C_{ps} V_s}{M_{H_2} V_{MH}^2 \left(V_g C_{pg} x_1 + V_s C_{ps} x_2\right)^3} - \frac{k_{amb}(u_2 - x_3) C_{ps} V_s}{V_{MH} \left(V_g C_{pg} x_1 + V_s C_{ps} x_2\right)^2} \cdot \Big[\frac{R u_1}{M_{H_2} V_g} - \frac{x_1 R k_{amb}}{M_{H_2} V_{MH} \left(V_g C_{pg} x_1 + V_s C_{ps} x_2\right)}\Big],$$

$$*_6 = \frac{2 k_{amb}(u_2 - x_3) C_{pg} u_1 C_{ps} V_s}{V_{MH} (V_g C_{pg} x_1 + V_s C_{ps} x_2)^3} + \frac{2 {k_{amb}}^2 (u_2 - x_3) C_{ps} V_s}{{V_{MH}}^2 (V_g C_{pg} x_1 + V_s C_{ps} x_2)^3},$$

It can be noted that the temperature of the MH tank is given in Kelvin, so x_3 is always positive and $\frac{x_3 R}{M_{H_2}} \neq 0$. In addition, we can note that only when $x_3 = T_{amb}$, the values of $*_3, *_4, *_5, *_6$ are zero and under this scenario, the rank of matrix $J_{f_r=0}$ is not full rank, then the MH tank system is non-observable. In contrast, when $x_3 \neq T_{amb}$, at least one of the values of $*_3, *_4, *_5, *_6$ is not zero and the rank of matrix $J_{f_r=0}$ is full rank, then the MH tank system is observable.

2) Case 2: $f_r \neq 0$

To check if the matrix J is full range, we consider its 3-order submatrix:

$$\begin{bmatrix} \frac{\partial y_1}{\partial x_1} & \frac{\partial y_1}{\partial x_2} & \frac{\partial y_1}{\partial x_3} \\ \frac{\partial \dot{y}_1}{\partial x_1} & \frac{\partial \dot{y}_1}{\partial x_2} & \frac{\partial \dot{y}_1}{\partial x_3} \\ \frac{\partial y_2}{\partial x_1} & \frac{\partial y_2}{\partial x_2} & \frac{\partial y_2}{\partial x_3} \end{bmatrix} = \begin{bmatrix} \frac{\partial y_1}{\partial x_1} & \frac{\partial y_1}{\partial x_2} & \frac{\partial y_1}{\partial x_3} \\ \frac{\partial \dot{y}_1}{\partial x_1} & \frac{\partial \dot{y}_1}{\partial x_2} & \frac{\partial \dot{y}_1}{\partial x_3} \\ 0 & 0 & 1 \end{bmatrix}. \tag{17}$$

In our previous work [6], we already showed that the following matrix

$$M = \begin{bmatrix} \frac{\partial y_1}{\partial x_1} & \frac{\partial y_1}{\partial x_2} \\ \frac{\partial \dot{y}_1}{\partial x_1} & \frac{\partial \dot{y}_1}{\partial x_2} \end{bmatrix},$$

is full rank, when $f_r \neq 0$. Therefore, the 3-order submatrix of the matrix (17) is also full rank. Consequently, the matrix J satisfies the full rank condition when $f_r \neq 0$, and we conclude that the MH tank system is observable when $f_r \neq 0$.

In summary, from an observability perspective, the area specified by the potential values of $[x_1, x_2, x_3]$ can be categorized into these three distinct regions:

$\Omega_1 = \{(\mathbf{x}, \mathbf{u}) \in \mathcal{X} \times \mathcal{U} \,|\, P > P_{eq,a}\}$, inst. obs.

$\Omega_2 = \{(\mathbf{x}, \mathbf{u}) \in \mathcal{X} \times \mathcal{U} \,|\, P_{eq,d} \leq P \leq P_{eq,a}, x_3 = T_{amb}\}$, non-obs.

$\Omega_3 = \{(\mathbf{x}, \mathbf{u}) \in \mathcal{X} \times \mathcal{U} \,|\, P_{eq,d} \leq P \leq P_{eq,a}, x_3 \neq T_{amb}\}$, inst. obs.

$\Omega_4 = \{(\mathbf{x}, \mathbf{u}) \in \mathcal{X} \times \mathcal{U} \,|\, P < P_{eq,d}\}$. inst. obs.

It is important to mention that the areas can likewise be described equivalently using f_r in this manner:

$$\Omega_1 = \{(\mathbf{x}, \mathbf{u}) \in \mathcal{X} \times \mathcal{U} |\ f_r > 0\}, \quad \text{inst. obs}$$

$$\Omega_2 = \{(\mathbf{x}, \mathbf{u}) \in \mathcal{X} \times \mathcal{U} |\ f_r = 0, x_3 = T_{amb}\}, \quad \text{non-obs}$$

$$\Omega_3 = \{(\mathbf{x}, \mathbf{u}) \in \mathcal{X} \times \mathcal{U} |\ f_r = 0, x_3 \neq T_{amb}\}, \quad \text{inst. obs}$$

$$\Omega_1 = \{(\mathbf{x}, \mathbf{u}) \in \mathcal{X} \times \mathcal{U} |\ f_r < 0\}, \quad \text{inst. obs}$$

Remark 1. *Although there still exists a non-observable region in the three-order state-space model, different from the observability analysis of the two-order state-space model discussed in our previous works [6], [7], we emphasize that the non-observable region is more difficult to reach since it requires the exact equality $T = T_{amb}$, which will not be satisfied in common operating modes due to the exothermic and endothermic reactions of the system.*

Remark 2. *The non-observability in the domain Ω_2 comes from the fact that $\dot{\mathbf{x}} = 0$ in this region. Therefore, the system dynamics does not depend on the states at this point, and no observability property can be guaranteed.*

IV. Observer design of the MH tank model

A. Proposal

We consider again the input-affine nonlinear system (11). Moreover, assume that system (11) is forward invariant and has a unique solution in a compact set $\mathbf{X} \subsetneq \mathbb{R}^n$ uniformly for all $\mathbf{u} \in \mathbf{U} \subsetneq \mathbb{R}^m$ where $\mathbf{U}$ is also a compact set.

Based on recent results on high-gain observers for multi-input multi-output systems [12], we introduce the following assumption, which will be used in the observer design.

Assumption 1. *There exist C^1 functions $\mathbf{\Phi}_\sigma : \mathcal{X} \to \mathbb{R}^n$, matrices $\mathbf{L}, \mathbf{M} \in \mathbb{R}^{n \times n}$ (both invertible), $\mathbf{N} \in \mathbb{R}^{p \times p}$, and*

$\mathbf{C} \in \mathbb{R}^{p\times n}$, *where* $\mathbf{L}$, $\mathbf{M}$, *and* $\mathbf{N}$ *depend on the observer gain* l. *In addition, there exist matrix functions* $\mathbf{u} \mapsto \mathbf{K}(\mathbf{u}) \in \mathbb{R}^{n\times p}$ *and* $\mathbf{u} \mapsto \mathbf{A}(\mathbf{u}) \in \mathbb{R}^{n\times n}$, *together with a symmetric positive definite matrix* $\mathbf{P}_\eta \in \mathbb{R}^{n\times n}$, *such that*

O1) the mappings $\mathbf{\Phi}_\sigma$ *are diffeomorphism on* $\mathcal{X}$,

O2) $\mathbf{C}\mathbf{\Phi}_\sigma(\mathbf{x}) = \mathbf{h}(\mathbf{x})$,

O3) for any $\mathbf{u}$, *the following conditions are satisfied:*

$$\mathbf{P}_\eta(\mathbf{A}(\mathbf{u}) - \mathbf{K}(\mathbf{u})\mathbf{C}) + (\mathbf{A}(\mathbf{u}) - \mathbf{K}(\mathbf{u})\mathbf{C})^\top \mathbf{P}_\eta \le -2\gamma \mathbf{P}_\eta,$$
$$\mathbf{A}(\mathbf{u})\mathbf{L} = \mathbf{L}\mathbf{M}\mathbf{A}(\mathbf{u}), \quad \mathbf{N}\mathbf{C}\mathbf{L} = \mathbf{C}.$$

Moreover, there exists a scalar δ *satisfying*

O4) $\lim_{l\to+\infty} \delta = 0$,

O5) For all $\mathbf{x}_a \in \mathfrak{C}$, $\mathbf{x}_b \in \hat{\mathfrak{C}}$ *and* $\mathbf{u} \in \mathcal{U}$,

$$\left|\mathbf{P}_\eta^{\frac{1}{2}}\mathbf{M}^{-1}\mathbf{L}^{-1}[\mathbf{B}(\mathbf{\Phi}_\sigma(\mathbf{x}_a),\mathbf{u}) - \mathbf{B}(\mathbf{\Phi}_\sigma(\mathbf{x}_b),\mathbf{u})]\right| \le \delta \left|\mathbf{P}_\eta^{\frac{1}{2}}\mathbf{L}^{-1}[\mathbf{\Phi}_\sigma(\mathbf{x}_a) - \mathbf{\Phi}_\sigma(\mathbf{x}_b)]\right|$$

is satisfied where the function $\mathbf{B} : \mathbb{R}^{n\times m} \to \mathbb{R}^n$ *are defined as*

$$\mathbf{B}(\mathbf{\Phi}_\sigma(\mathbf{x}),\mathbf{u}) = L_\mathbf{f}\mathbf{\Phi}_\sigma(\mathbf{x}) + L_\mathbf{g}\mathbf{\Phi}_\sigma(\mathbf{x})\mathbf{u} - \mathbf{A}(\mathbf{u})\mathbf{\Phi}_\sigma(\mathbf{x}).$$

Following the representation in [7], the MH tank model (1a) and (1b) can be rewritten as the following input-affine nonlinear switched system:

$$\begin{aligned}\dot{\mathbf{x}} &\coloneqq \mathbf{f}_\sigma(\mathbf{x},\mathbf{u}) = \mathbf{f}_\sigma(\mathbf{x}) + \mathbf{g}(\mathbf{x})\mathbf{u},\\ \mathbf{y} &\coloneqq \mathbf{h}(\mathbf{x}),\end{aligned} \tag{18}$$

where σ is a switching signal for system dynamics $\mathbf{f}$ with the index set $\mathcal{G} \coloneqq \{1,2,3,4\}$ that is equal to s when $(\mathbf{x},\mathbf{u}) \in \Omega_s$, and Ω_s denotes the different modes of operation defined at the end of Section III. The vector fields $\mathbf{f}_s$ with $s \in \mathcal{G}$ and $\mathbf{g}$ are defined as

$$\mathbf{f}_1(\mathbf{x}) = \begin{bmatrix} -\frac{f_{r,a}}{V_g} \\ \frac{f_{r,a}}{V_s} \\ \frac{f_{r,a}\frac{\Delta H_a}{M_{H_2}} + f_{r,a}x_3(C_{pg}-C_{ps}) - \frac{k_{amb}\cdot x_3}{V_{MH}}}{V_gC_{pg}x_1 + V_sC_{ps}x_2} \end{bmatrix},$$

$$\mathbf{f}_2(\mathbf{x}) = \begin{bmatrix} 0 \\ 0 \\ \frac{-k_{amb}\cdot T_{amb}}{V_{MH}(V_gC_{pg}x_1 + V_sC_{ps}x_2)} \end{bmatrix},$$

$$\mathbf{f}_3(\mathbf{x}) = \begin{bmatrix} 0 \\ 0 \\ -\frac{k_{amb}\cdot x_3}{V_{MH}} \\ \frac{}{V_gC_{pg}x_1 + V_sC_{ps}x_2} \end{bmatrix},$$

$$\mathbf{f}_4(\mathbf{x}) = \begin{bmatrix} -\frac{f_{r,d}}{V_g} \\ \frac{f_{r,d}}{V_s} \\ \frac{f_{r,d}\frac{\Delta H_d}{M_{H_2}} + f_{r,d}x_3(C_{pg}-C_{ps}) - \frac{k_{amb}\cdot x_3}{V_{MH}}}{V_gC_{pg}x_1 + V_sC_{ps}x_2} \end{bmatrix},$$

$$\mathbf{g}(\mathbf{x}) = \begin{bmatrix} \frac{1}{V_g} & 0 \\ 0 & 0 \\ 0 & \frac{k_{amb}}{V_{MH}(V_gC_{pg}x_1 + V_sC_{ps}x_2)} \end{bmatrix}.$$

Then we can design the observer as

$$\begin{aligned}\dot{\hat{\mathbf{x}}} &\coloneqq \mathbf{F}_s(\hat{\mathbf{x}},\mathbf{h},\mathbf{u}) = \mathbf{f}_\sigma(\hat{\mathbf{x}}) + \mathbf{g}(\hat{\mathbf{x}})\mathbf{u}\\ &\quad + s_{f_r}\cdot\left[\frac{\partial \mathbf{\Phi}_\sigma(\hat{\mathbf{x}})}{\partial \mathbf{x}}\right]^{-1}\mathbf{L}\mathbf{M}\mathbf{K}\mathbf{N}[\mathbf{h}(\mathbf{x}) - \mathbf{h}(\hat{\mathbf{x}})],\end{aligned} \tag{19}$$

where s_{f_r} is the time-varying switching function:

$$s_{f_r}(t) = \begin{cases} 0, & |\text{if } \hat{f}_r| < \epsilon_{tol} \text{ and } \hat{x}_3 = T_{amb} \\ 1, & otherwise. \end{cases} \tag{20}$$

$\epsilon_{tol} > 0$ is the tunable tolerance of $\hat{f}_r$. Notice that even if the estimation of the observer $\hat{\mathbf{x}}$ is not the same as the true one $\mathbf{x}$, the observer still has the same operating mode σ. An explanation on how to achieve this is provided in Section IV-B.

For the cases $s_{f_r} = 1$, the following lemma establishes the exponential convergence of the proposed observer.

Lemma 1. *Consider system* (18) *together with observer* (19), *and assume that Assumption* (1) *is satisfied. Furthermore, suppose that* $\hat{\mathbf{x}}(t) \in \mathcal{X}$ *for all* $t \ge 0$. *Then, for each mode* $\sigma \in \mathcal{G}\setminus\{2\}$, *there exists constants a, b,* $L_{\mathbf{\Phi}}$, $L_{\mathbf{\Phi}^{-1}}$, *such that*

$$\|\mathbf{x}(t) - \hat{\mathbf{x}}(t)\| \le L_{\mathbf{\Phi}^{-1}}L_{\mathbf{\Phi}}ae^{-bt}\|\mathbf{x}(0) - \hat{\mathbf{x}}(0)\|. \tag{21}$$

The proof is postponed to Appendix A.

For the case $s_{f_r} = 0$, observer (19) reduces to the following open-loop system

$$\dot{\hat{\mathbf{x}}} = \mathbf{f}_2(\hat{\mathbf{x}}) + \mathbf{g}(\hat{\mathbf{x}})\mathbf{u}. \tag{22}$$

In this case, the error dynamics of $\mathbf{x}$ is

$$\dot{\tilde{\mathbf{x}}} = \dot{\mathbf{x}} - \dot{\hat{\mathbf{x}}} = \mathbf{f}_2(\mathbf{x}) + \mathbf{g}(\mathbf{x})\mathbf{u} - \mathbf{f}_2(\hat{\mathbf{x}}) - \mathbf{g}(\hat{\mathbf{x}})\mathbf{u} = 0. \tag{23}$$

As a result, the estimation error remains constant within this region. It follows that if the system does not remain in the region $\Omega_2$for an extended period, exponential convergence of the observer can still be ensured. This result can be described by the following theorem.

Theorem 1. *Consider system* (18), *observer* (19) *and assume that* $\hat{\boldsymbol{x}}(t) \in \mathcal{X}$ *for all* $t \ge 0$ *and that Assumption 1 holds. Moreover, denote by* $T_s(t_i,t_{i+1})$ *the sum of the total time that* $\sigma(t) = s$ *in the interval* $[t_i,t_{i+1})$. *Then, for any switching signal* $\sigma : [0,\infty) \to \mathcal{G}$ *and corresponding switching instants* $\mathfrak{G} \coloneqq \{t_1,t_2,\ldots,t_k,\ldots\}$ *such that*

$$T_1(0,t) + T_3(0,t) + T_4(0,t) \ge \varpi t, \quad \forall t \ge 0 \tag{24}$$

holds for some constants $0 < \underline{\varpi} \leq 1$ *and* $t_1 \geq 0$*, we have*

$$\|\mathbf{x}(t) - \hat{\mathbf{x}}(t)\| \leq \prod_{k=0}^{i-1} (L_{\mathbf{\Phi}^{-1}} L_{\mathbf{\Phi}} a) \cdot e^{-b\underline{\varpi}t} \cdot \|\mathbf{x}(0) - \hat{\mathbf{x}}(0)\|.$$

for all $t \geq 0$*.*

The proof is postponed to Appendix B.

B. On synchronizing the switching between the observer and the plant

In the MH tank system, a lack of synchronization between the observer and the plant may cause the observer to evolve according to incorrect dynamics, which degrade the accuracy of state estimation. Therefore, ensuring that the observer (19) operates under the same mode σ as the system is essential. According to (3), the mode of the system can be determined from the sign of f_r. In our earlier study [6], we presented a simple estimator, namely the unknown system dynamic estimator (USDE), to evaluate f_r, and its construction is therefore omitted here:

$$\hat{f}_r = u_{1f} - V_g \cdot \frac{\bar{x}_1 - \bar{x}_{1f}}{\kappa}. \tag{25}$$

where $\bar{x}_1$ can be obtained from (1b) as

$$\bar{x}_1 \triangleq \frac{y_1 \cdot M_{H_2}}{R \cdot y_2}, \tag{26}$$

and $(\cdot)_f = [\cdot]/(\kappa s + 1)$ is the low-pass filter operation, with $\kappa > 0$ a filter parameter.

Taking this into account, we propose the following switching mechanism for the observer:

$$\dot{\hat{\mathbf{x}}} = \begin{cases} \mathbf{f}_1(\hat{\mathbf{x}}) + \mathbf{g}(\hat{\mathbf{x}})\,\mathbf{u} + \mathbf{\Pi}_1, & \hat{f}_r > \epsilon_{tol}, \\ \mathbf{f}_2(\hat{\mathbf{x}}) + \mathbf{g}(\hat{\mathbf{x}})\,\mathbf{u}, & \left|\hat{f}_r\right| \leq \epsilon_{tol}, \hat{x}_3 = T_{amb}, \\ \mathbf{f}_3(\hat{\mathbf{x}}) + \mathbf{g}(\hat{\mathbf{x}})\,\mathbf{u} + \mathbf{\Pi}_3, & \left|\hat{f}_r\right| \leq \epsilon_{tol}, \hat{x}_3 \neq T_{amb}, \\ \mathbf{f}_4(\hat{\mathbf{x}}) + \mathbf{g}(\hat{\mathbf{x}})\,\mathbf{u} + \mathbf{\Pi}_4, & \hat{f}_r < -\epsilon_{tol}, \end{cases} \tag{27}$$

where

$$\mathbf{\Pi}_\sigma = \left[\frac{\partial \mathbf{\Phi}_\sigma(\hat{\mathbf{x}})}{\partial \mathbf{x}}\right]^{-1} \mathbf{LMKN}[\mathbf{h}(\mathbf{x}) - \mathbf{h}(\hat{\mathbf{x}})]$$

with $\sigma = \{1, 3, 4\}$ and ϵ_{tol} is a positive threshold included to consider potential errors during the estimation of f_r.

C. Robustness to de-synchronization

Naturally, since the true mode of the plant is not directly measured, but estimated through (25), there can be some time ranges where the mode of the observer and the plant are not the same, thus they are de-synchronized. Nonetheless, since the observer is exponentially stable, it exhibits robustness to discrepancies between the plant and the model. As a result, if the desynchronization time is sufficiently short, asymptotic convergence of the form (9) is still achieved. The remainder of this section provides further details about this behavior. We have the following theorem:

Table I: Optimal values with multi-object identification [13]

Parameter	Value	Unit
ΔH_a	20000	J/mol
ΔS_d	109	J/(mol · K)
ΔH_d	25530	J/mol
φ	0.3228	-
φ_0	0	-
β	0.1333	-
C_a	388.6084	1/s
C_d	2761.0	1/s
E_a	30847	J/mol
E_d	32507	J/mol
k_{amb}	1.2138	J/(K · s)
C_{ps}	6425.6	J/(kg · K)
ρ_{s0}	6247.0	kg/m^3
ε	0.6928	-
V_{MH}	$3 \cdot 10^{-4}$	m^3

Table II: Thermodynamic model and remaining parameters [14].

Symbol	Value	Symbol	Value
m_{total}	0.0315 kg	T_{amb}	298.15 K
k_p	0.1537		

Theorem 2. *Consider the plant* (18) *and observer* (19)*, and assume that the observer mode* σ_j *satisfies condition* (24) *and the hypotheses of Theorem 1. Suppose that the plant and observer modes satisfy* $\sigma_i \neq \sigma_j$ *for* $t \in [t_1, t_2)$ *and* $\sigma_i = \sigma_j$ *for all* $t \geq t_2$*. Then:*

1) *The estimation error* $\tilde{\mathbf{x}}(t) = \mathbf{x}(t) - \hat{\mathbf{x}}(t)$ *remains bounded for all* $t \in [t_1, t_2)$*.*
2) *For all* $t \geq t_2$*, the estimation error converges exponentially.*

The proof is postponed to Appendix C.

V. Numerical simulations

In this section, a numerical simulation is carried out to verify the feasibility of the proposed observation scheme. The parameters listed in Table I are used, with additional parameters provided in Table II.

One of the system inputs, namely the normalized mass-flow rate, f_{in}, is presented in Fig. 1. The other input, i.e., the ambient temperature, T_{amb}, is assumed to remain constant. $f_{in} > 0$ corresponds to charge while $f_{in} < 0$ corresponds to discharge. The system initial conditions are set as: initial temperature $T(0) = 298.15\,\mathrm{K}$, $x_1(0) = 0.0824\,\mathrm{kg/m^3}$, $x_2(0) = 6270.6\,\mathrm{kg/m^3}$, $x_3(0) = 298.15\,\mathrm{K}$ and the initial conditions of the observer are $\hat{x}_1(0) = 0.5\,\mathrm{kg/m^3}$, $\hat{x}_2(0) = 6260\,\mathrm{kg/m^3}$, $\hat{x}_3(0) = 300\,\mathrm{K}$. The low-pass filter parameter κ in (25) is fixed to $\kappa = 1 \cdot 10^{-2}$ and the threshold in (27) is chosen as $\epsilon_{tol} = 1 \cdot 10^{-5}$. Furthermore, observer gain $l = 4$ and $\mathbf{L}, \mathbf{M}, \mathbf{N}, \mathbf{K}$ are defined as

$$\mathbf{L} = \mathrm{diag}(1, 1, 4), \quad \mathbf{M} = \mathrm{diag}(4, 4, 4),$$

$$\mathbf{N} = \mathrm{diag}(1, 1), \quad \mathbf{K} = \begin{pmatrix} 0.3596 & 0 \\ 0 & 1.3155 \\ 0 & 0.4298 \end{pmatrix}. \tag{28}$$

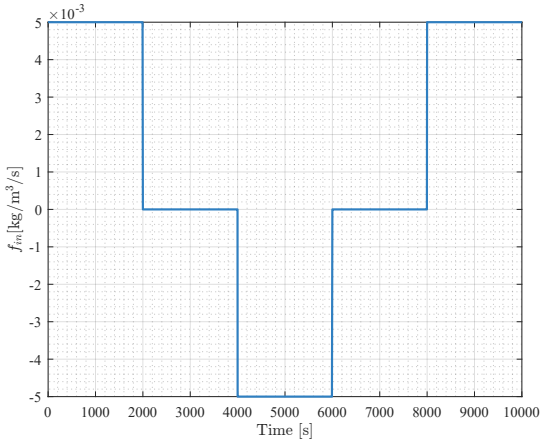

Fig. 1. Evolution of f_{in} for the system (18).

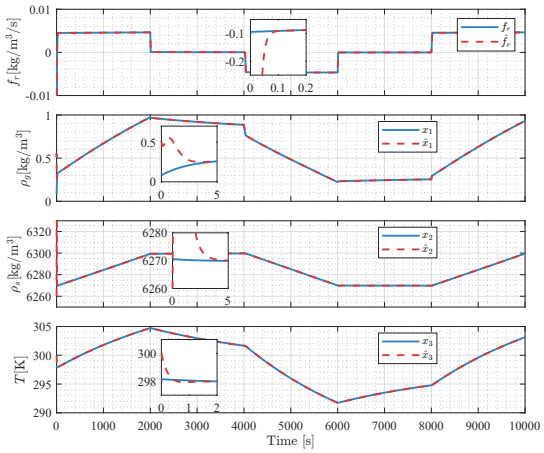

Fig. 2. USDE and observer results in simulation.

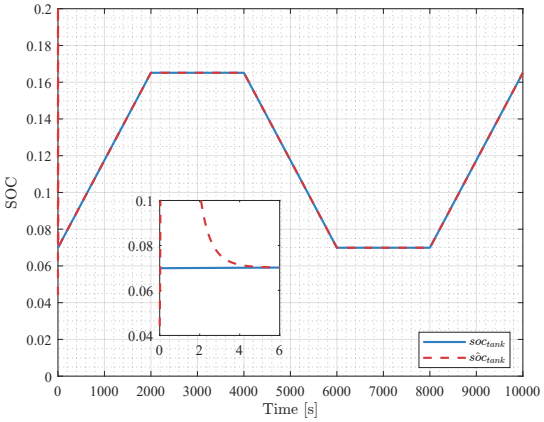

Fig. 3. Comparison between SOC estimates and true values in simulation.

The simulation results are presented in Fig. 2. From this figure, we can see that the estimation of the sorption rate $\hat{f}_r$ converges quickly within $0.2\,\mathrm{s}$, the estimations $\hat{x}_1$ and $\hat{x}_2$ converge within the first $5\,\mathrm{s}$, while the estimation $\hat{x}_3$ converges within $2\,\mathrm{s}$.

Finally, the SOC estimate, $\hat{soc}_{tank}$ is displayed in Fig. 3. It can be observed that the SOC estimate follows the same trend as the estimate of x_2 and converges within $6\,\mathrm{s}$.

VI. Experimental validation

The proposed observer and SOC estimation SOC estimation approach have been experimentally validated using a real setup (Fig. 4). The experimental platform includes a commercial MH tank (H2planet® MyH2 SLIM 350) based on Hydralloy C5 ($Ti_{0.95}Zr_{0.05}Mn_{1.48}Fe_{0.08}Al_{0.01}$), along with hydrogen pipelines and measurement devices such as mass flow meters, pressure sensors, and thermocouples. The MH tank is naturally cooled in the ambient environment. All sensor signals are collected and processed in real time using an NI sbRIO-9629 platform, providing the experimental data required for parameter identification and SOC estimation validation. The

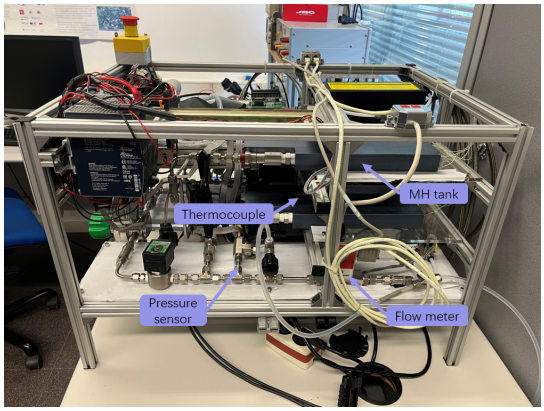

Fig. 4. Diagram of experimental setup [6]

profiles of the measured variables during the experiment are depicted in Fig. 5, including the pipe pressure p_{pipe}, tank temperature T, and flow rate F_{in}.

The low-pass filter parameter κ in (25) is fixed to $\kappa = 1.5$ and the threshold in (27) is chosen as $\epsilon_{tol} = 1 \cdot 10^{-5}$. For the absorption process, the observer is initialized with $\hat{x}_1(0) = 0.5\,\mathrm{kg/m^3}$ and $\hat{x}_2(0) = 6260\,\mathrm{kg/m^3}$. Furthermore, the observer gain l and the matrices $\mathbf{L}$, $\mathbf{M}$, $\mathbf{N}$, and $\mathbf{K}$ are chosen to be the same as those in (28).

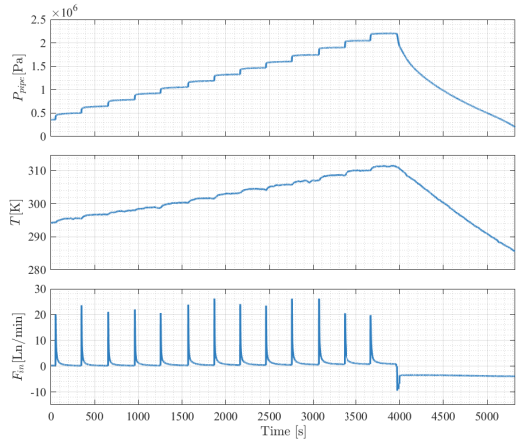

Fig. 5. Experiment measurable variables: pipe pressure P_{pipe}, tank temperature T and flow rate F_{in}.

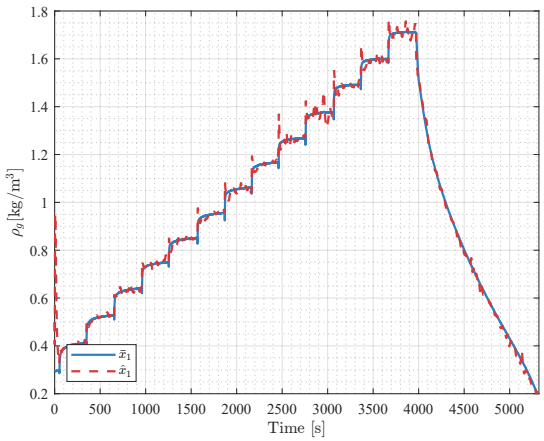

Fig. 6. Observer results obtained for the experimental results (ρ_g).

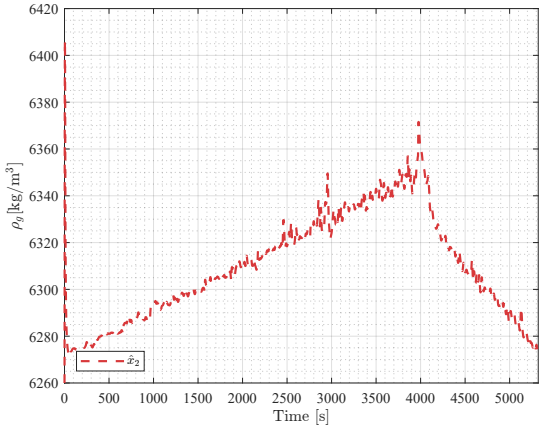

Fig. 7. Experimental validation of the observer for (ρ_s).

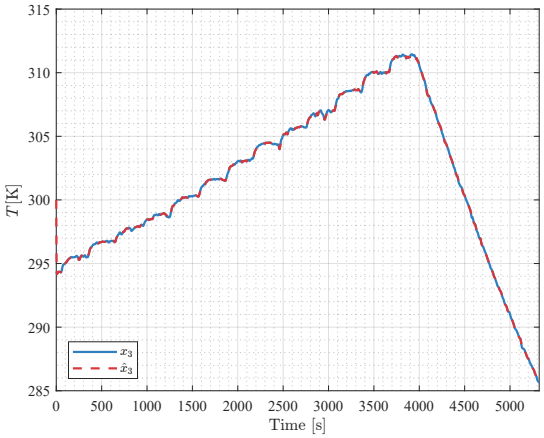

Fig. 8. Observer results obtained for the experimental results (T).

Fig. 6 illustrates the evolution of the estimate of ρ_g. It can be seen that the estimate $\hat{x}_1$ converges within 100s. Additionally, Fig. 7 depicts the evolution of the estimate of ρ_s. Since the true trajectory of ρ_s can not be directly measured by sensors, it is not included in the figure. Fig. 8 illustrates the evolution of the estimate of T. The results indicate that the estimate closely follows the true trajectory of the tank temperature T.

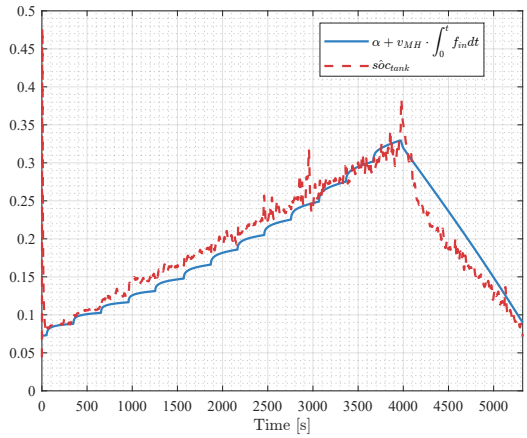

Fig. 9. SOC estimation: comparison of observer-based and offline results.

Finally, Fig. 9 illustrates the evolution of the SOC estimate, $\hat{soc}_{tank}$. Since $\hat{x}1$ and $\hat{x}_2$ are used to compute $\hat{soc}_{tank}$, its convergence behavior is inherently influenced by the convergence properties of both $\hat{x}1$ and $\hat{x}_2$. (10) is employed to estimate soc_{tank}, given that its true value is not directly measurable. The initial value of soc_{tank}, namely $m_{H_2}(0)$, is unknown. Hence, a posteriori parameter α is determined using the PCT curve. The figure shows that $\hat{soc}_{tank}$ converges to the true soc_{tank}, confirming the effectiveness of the proposed SOC estimation method.

VII. Conclusion

This paper proposed a nonlinear switching high-gain observer for SOC estimation in MH storage tanks, addressing the intrinsic non-observability arising in the equilibrium region between hydrogen absorption and desorption. The observability properties of a three-order MH tank model are analyzed, showing that, compared with commonly used two-order models, the non-observable region is significantly reduced. Based on this model and its observability analysis, a switched high-gain observer is designed to ensure fast and accurate state estimation in observable regions. Sufficient conditions for observer convergence are established under synchronous switching, and robustness to observer–plant de-synchronization is demonstrated. The proposed SOC estimation framework is shown to be effective and practically relevant through both numerical simulations and experimental validation.

Appendix A
Proof of Lemma 1

From the observability analysis of Section III, we have that, for each mode $\sigma \in \mathcal{G}\setminus\{2\}$, there exists a function $\mathbf{\Phi}_\sigma$, defined as [15, Section 7.2]

$$\mathbf{\Phi}_\sigma(\mathbf{x}) = \begin{bmatrix} \mathbf{\Phi}_{\sigma 1}(\mathbf{x}) & \cdots & \mathbf{\Phi}_{\sigma p}(\mathbf{x}) \end{bmatrix}^\top,$$

$$\mathbf{\Phi}_{\sigma i}(x) = \begin{bmatrix} \mathbf{h}_i(\mathbf{x}) & L_{\mathbf{f}_\sigma}\mathbf{h}_i(x) & \cdots & L_{\mathbf{f}_\sigma}^{p_i-1}\mathbf{h}_i(\mathbf{x}) \end{bmatrix}^\top$$

where $\mathbf{h}_i$ is the i-th component of $\mathbf{h}$, p_i are observability indexes and $\sum_{i=1}^{p} p_i = n$. Let $\eta_\sigma = \mathbf{\Phi}_\sigma(\mathbf{x}), \hat{\eta}_\sigma = \mathbf{\Phi}_\sigma(\hat{\mathbf{x}}), \tilde{\eta}_\sigma = \eta_\sigma - \hat{\eta}_\sigma$, then the system can be transformed from $\mathbf{x}$-coordinate

to η-coordinate. Now the system dynamics in η-coordinate can be rewritten as

$$\begin{aligned}\dot{\eta}_\sigma &= \frac{\partial \mathbf{\Phi}_\sigma(\mathbf{x})}{\partial \mathbf{x}}\dot{\mathbf{x}} = L_{\mathbf{f}_\sigma}\mathbf{\Phi}_\sigma(\mathbf{x}) + L_{\mathbf{g}}\mathbf{\Phi}_\sigma(\mathbf{x})\mathbf{u} \\ &= L_{\mathbf{f}_\sigma}\mathbf{\Phi}_\sigma(\mathbf{x}) + L_{\mathbf{g}}\mathbf{\Phi}_\sigma(\mathbf{x})\mathbf{u} - \mathbf{A}(\mathbf{u})\mathbf{\Phi}_\sigma(\mathbf{x}) \\ &\quad + \mathbf{A}(\mathbf{u})\mathbf{\Phi}_\sigma(\mathbf{x}) \\ &= \mathbf{A}(\mathbf{u})\eta_\sigma + \mathbf{B}(\eta_\sigma, \mathbf{u}),\end{aligned} \tag{29}$$

$$\begin{aligned}\dot{\hat{\eta}}_\sigma &= \frac{\partial \mathbf{\Phi}_\sigma(\hat{\mathbf{x}})}{\partial \mathbf{x}}\dot{\hat{\mathbf{x}}} = L_{\mathbf{f}_\sigma}\mathbf{\Phi}_\sigma(\hat{\mathbf{x}}) + L_{\mathbf{g}}\mathbf{\Phi}_\sigma(\hat{\mathbf{x}})\mathbf{u} \\ &\quad + \mathbf{LMK}(\mathbf{u})\mathbf{NC}(\eta_\sigma - \hat{\eta}_\sigma) \\ &= L_{\mathbf{f}_\sigma}\mathbf{\Phi}_\sigma(\hat{\mathbf{x}}) + L_{\mathbf{g}}\mathbf{\Phi}_\sigma(\hat{\mathbf{x}})\mathbf{u} \\ &\quad + \mathbf{LMK}(\mathbf{u})\mathbf{NC}(\eta_\sigma - \hat{\eta}_\sigma) - \mathbf{A}(\mathbf{u})\mathbf{\Phi}_\sigma(\hat{\mathbf{x}}) \\ &\quad + \mathbf{A}(\mathbf{u})\mathbf{\Phi}_\sigma(\hat{\mathbf{x}}) \\ &= \mathbf{A}(\mathbf{u})\hat{\eta}_\sigma + \mathbf{B}(\hat{\eta}_\sigma, \mathbf{u}) + \mathbf{LMK}(\mathbf{u})\mathbf{NC}(\eta_\sigma - \hat{\eta}_\sigma).\end{aligned} \tag{30}$$

Define Lyapunov function in η coordinate, $V_\sigma(\eta_\sigma) = \frac{1}{2}\tilde{\eta}_\sigma^\top \left[\mathbf{LMP}_\eta^{-1}\mathbf{L}^\top\right]^{-1}\tilde{\eta}_\sigma$, the derivative of $V_\sigma(\eta_\sigma)$ is

$$\begin{aligned}\dot{V}_\sigma(\eta) &= \tilde{\eta}_\sigma^\top \mathbf{L}^{-\top}\mathbf{P}_\eta\mathbf{M}^{-1}\mathbf{L}^{-1}\dot{\tilde{\eta}}_\sigma \\ &= \tilde{\eta}_\sigma^\top \mathbf{L}^{-\top}\mathbf{P}_\eta\mathbf{M}^{-1}\mathbf{L}^{-1} \\ &\quad \cdot \left[(\mathbf{A} - \mathbf{LMKNC})\tilde{\eta}_\sigma + \mathbf{B}(\eta_\sigma, \mathbf{u}) - \mathbf{B}(\hat{\eta}_\sigma, \mathbf{u})\right].\end{aligned}$$

Based on O3) and O5),

$$\begin{aligned}&\dot{V}_\sigma(\eta_\sigma) = \left(\mathbf{L}^{-1}\tilde{\eta}_\sigma\right)^\top \mathbf{P}_\eta\mathbf{M}^{-1}\mathbf{L}^{-1} \\ &\cdot \left[(\mathbf{AL} - \mathbf{LMKNCL})\cdot\mathbf{L}^{-1}\tilde{\eta}_\sigma + \mathbf{B}(\eta_\sigma, \mathbf{u}) - \mathbf{B}(\hat{\eta}_\sigma, \mathbf{u})\right] \\ &= \left(\mathbf{L}^{-1}\tilde{\eta}_\sigma\right)^\top \cdot [\mathbf{P}_\eta\mathbf{M}^{-1}\mathbf{L}^{-1}(\mathbf{AL} - \mathbf{LMKNCL})\cdot\mathbf{L}^{-1}\tilde{\eta}_\sigma \\ &+ \mathbf{P}_\eta\mathbf{M}^{-\mathbf{1}}\mathbf{L}^{-\mathbf{1}}(\mathbf{B}(\eta_\sigma, \mathbf{u}) - \mathbf{B}(\hat{\eta}_\sigma, \mathbf{u}))] \\ &= \left(\mathbf{L}^{-1}\tilde{\eta}_\sigma\right)^\top \cdot [(\mathbf{P}_\eta\mathbf{A} - \mathbf{P}_\eta\mathbf{KC})\cdot\mathbf{L}^{-1}\tilde{\eta}_\sigma \\ &+ \mathbf{P}_\eta\mathbf{M}^{-\mathbf{1}}\mathbf{L}^{-\mathbf{1}}(\mathbf{B}(\eta_\sigma, \mathbf{u}) - \mathbf{B}(\hat{\eta}_\sigma, \mathbf{u}))] \\ &= \left(\mathbf{L}^{-1}\tilde{\eta}_\sigma\right)^\top \cdot (\mathbf{P}_\eta\mathbf{A} - \mathbf{P}_\eta\mathbf{KC})\cdot\mathbf{L}^{-1}\tilde{\eta}_\sigma \\ &+ \left(\mathbf{L}^{-\mathbf{1}}\tilde{\eta}_\sigma\right)^\top \mathbf{P}_\eta\mathbf{M}^{-\mathbf{1}}\mathbf{L}^{-\mathbf{1}}[\mathbf{B}(\eta_\sigma, \mathbf{u}) - \mathbf{B}(\hat{\eta}_\sigma, \mathbf{u})] \\ &\leq -\gamma\left|\mathbf{P}_\eta^{\frac{1}{2}}\mathbf{L}^{-1}\tilde{\eta}_\sigma\right|^2 + \delta\left|\mathbf{P}_\eta^{\frac{1}{2}}\mathbf{L}^{-1}\tilde{\eta}_\sigma\right|^2.\end{aligned}$$

Since O4),

$$\dot{V}_\sigma(\eta_\sigma) \leq -\gamma\tilde{\eta}_\sigma^\top \mathbf{L}^{-\top}\mathbf{P}_\eta\mathbf{L}^{-1}\tilde{\eta}_\sigma \leq -\frac{\gamma}{2}\tilde{\eta}_\sigma^\top \mathbf{L}^{-\top}\mathbf{P}_\eta\mathbf{L}^{-1}\tilde{\eta}_\sigma.$$

Then as $\mathbf{P}_\eta \geq \lambda_{min}(\mathbf{P}_\eta), \mathbf{MP}_\eta^{-1} \geq \lambda_{min}\left(\mathbf{MP}_\eta^{-1}\right)$, we can get $\mathbf{P}_\eta = \mathbf{P}_\eta\mathbf{MP}_\eta^{-1}\mathbf{P}_\eta\mathbf{M}^{-1} \geq \lambda_{min}(\mathbf{P}_\eta)\lambda_{min}\left(\mathbf{MP}_\eta^{-1}\right)\mathbf{P}_\eta\mathbf{M}^{-1}$, so

$$\begin{aligned}\dot{V}_\sigma(\eta_\sigma) &\leq -\gamma\lambda_{min}(\mathbf{P}_\eta)\lambda_{min}\left(\mathbf{MP}_\eta^{-1}\right)\cdot\frac{1}{2}\tilde{\eta}_\sigma^\top \\ &\quad \cdot \mathbf{L}^{-\top}\mathbf{P}_\eta\mathbf{M}^{-\mathbf{1}}\mathbf{L}^{-1}\cdot\tilde{\eta}_\sigma \\ &= -\gamma\lambda_{min}(\mathbf{P}_\eta)\lambda_{min}\left(\mathbf{MP}_\eta^{-1}\right)\cdot V_\sigma(\eta_\sigma) \\ &= -qV_\sigma(\eta_\sigma).\end{aligned}$$

It can be concluded that, for each mode,

$$\|\eta(t) - \hat{\eta}(t)\| \leq ae^{-b(t)}\|\eta(0) - \hat{\eta}(0)\| \tag{31}$$

holds for all $t \geq 0$ with some constants $a, b > 0$.

Moreover, since the functions $\mathbf{\Phi}_\sigma(\mathbf{x})$ are diffeomorphisms on the set $\mathcal{X}$, there exist Lipschitz constants $L_{\mathbf{\Phi}}$ and $L_{\mathbf{\Phi}^{-1}}$ such that

$$\begin{aligned}&\|\mathbf{x}(t) - \hat{\mathbf{x}}(t)\| = \|\mathbf{\Phi}_\sigma^{-1}\left(\mathbf{\Phi}_\sigma\left(\mathbf{x}\right)\right) - \mathbf{\Phi}_\sigma^{-1}\left(\mathbf{\Phi}_\sigma\left(\hat{\mathbf{x}}\right)\right)\| \\ &\leq L_{\mathbf{\Phi}^{-1}}\|\mathbf{\Phi}_\sigma\left(\mathbf{x}\right) - \mathbf{\Phi}_\sigma\left(\hat{\mathbf{x}}\right)\| \\ &\leq L_{\mathbf{\Phi}^{-1}}ae^{-bt}\|\mathbf{\Phi}_\sigma\left(\mathbf{x}(0)\right) - \mathbf{\Phi}_\sigma\left(\hat{\mathbf{x}}(0)\right)\| \\ &\leq L_{\mathbf{\Phi}^{-1}}L_{\mathbf{\Phi}}ae^{-bt}\|\mathbf{x}(0) - \hat{\mathbf{x}}(0)\|.\end{aligned} \tag{32}$$

Appendix B
Proof of Theorem 1

For any $t \in [t_i, t_{i+1})$, considering Lemma 1, we have

$$\begin{aligned}&\|\mathbf{x}(t) - \hat{\mathbf{x}}(t)\| \leq \prod_{k=0}^{i-1}(L_{\mathbf{\Phi}^{-1}}L_{\mathbf{\Phi}}ae^{-b(t_{k+1}-t_k)}) \\ &\cdot \|\mathbf{x}(0) - \hat{\mathbf{x}}(0)\| \\ &= \prod_{k=0}^{i-1}(L_{\mathbf{\Phi}^{-1}}L_{\mathbf{\Phi}}a)\cdot\prod_{p\in\mathcal{G}}e^{-bT_s(t_0,t)}\cdot\|\mathbf{x}(0) - \hat{\mathbf{x}}(0)\| \\ &= \prod_{k=0}^{i-1}(L_{\mathbf{\Phi}^{-1}}L_{\mathbf{\Phi}}a)\cdot e^{-b(T_1(t_0,t)+T_3(t_0,t)+T_4(t_0,t))} \\ &\cdot \|\mathbf{x}(0) - \hat{\mathbf{x}}(0)\| \\ &\leq \prod_{k=0}^{i-1}(L_{\mathbf{\Phi}^{-1}}L_{\mathbf{\Phi}}a)\cdot e^{-b\underline{\varpi}(t-0)}\cdot\|\mathbf{x}(0) - \hat{\mathbf{x}}(0)\|.\end{aligned} \tag{33}$$

Appendix C
Proof of Theorem 2

The plant and observer satisfy

$$\dot{\mathbf{x}} = \mathbf{f}_{\sigma_i}(\mathbf{x}, \mathbf{u}), \quad \dot{\hat{\mathbf{x}}} = \mathbf{f}_{\sigma_j}(\hat{\mathbf{x}}, \mathbf{u}) + \mathbf{l}\big[\mathbf{h}(\mathbf{x}) - \mathbf{h}(\hat{\mathbf{x}})\big],$$

with $\sigma_i, \sigma_j \in \mathcal{G}$ and $\mathbf{l} = s_{f_r}\cdot\left[\frac{\partial\mathbf{\Phi}_\sigma(\hat{\mathbf{x}})}{\partial\mathbf{x}}\right]^{-1}\mathbf{LMKN}$. The error $\tilde{\mathbf{x}} = \mathbf{x} - \hat{\mathbf{x}}$ and its dynamics can be obtained as:

$$\begin{aligned}\dot{\tilde{\mathbf{x}}} &= \mathbf{f}_{\sigma_i}(\mathbf{x}, \mathbf{u}) - \mathbf{f}_{\sigma_j}\left(\hat{\mathbf{x}}, \mathbf{u}\right) - \mathbf{l}\left[\mathbf{h}(\mathbf{x}) - \mathbf{h}(\hat{\mathbf{x}})\right] \\ &= \mathbf{f}_{\sigma_j}(\mathbf{x}, \mathbf{u}) - \mathbf{f}_{\sigma_j}(\hat{\mathbf{x}}, \mathbf{u}) - \mathbf{l}\left[\mathbf{h}(\mathbf{x}) - \mathbf{h}(\hat{\mathbf{x}})\right] \\ &\quad + \boldsymbol{\delta}(\mathbf{x}, \mathbf{u}),\end{aligned} \tag{34}$$

where the mismatch disturbance is

$$\boldsymbol{\delta}(\mathbf{x}, \mathbf{u}) = \mathbf{f}_{\sigma_i}(\mathbf{x}, \mathbf{u}) - \mathbf{f}_{\sigma_j}(\mathbf{x}, \mathbf{u}).$$

If σ_j satisfies condition (24) and the hypothesis of Theorem 1 hold, then, the error dynamics (34) are exponentially stable when $\boldsymbol{\delta}(\mathbf{x}, \mathbf{u}) = 0$. Consequently, the error dynamics are input-to-state stable with respect to the additive perturbation $\boldsymbol{\delta}(\mathbf{x}, \mathbf{u})$ [16]. Note that $\boldsymbol{\delta}(\mathbf{x}, \mathbf{u})$ is continuous in both arguments and that $\mathbf{x}$ and $\mathbf{u}$ are bounded. Hence, $\boldsymbol{\delta}(\mathbf{x}, \mathbf{u})$ is bounded, which guarantees that the estimation error norm $|\tilde{\mathbf{x}}|$ remains bounded.

Suppose that the observer and the plant are not synchronized over a finite time interval $t \in [t_1, t_2)$, for some $t_1, t_2 \geq 0$, and are synchronized for all $t \geq t_2$. Then, the estimation error $\tilde{\mathbf{x}}$ remains bounded on $[t_1, t_2)$ and converges exponentially to zero for all $t \geq t_2$. Consequently, if the de-synchronization intervals are sufficiently short, the convergence property in (9) is preserved.

REFERENCES

[1] C. Tarhan and M. A. Çil, "A study on hydrogen, the clean energy of the future: Hydrogen storage methods," *Journal of Energy Storage*, vol. 40, p. 102676, 2021.

[2] V. Dusastre, *Materials for sustainable energy: a collection of peer-reviewed research and review articles from Nature Publishing Group*. World Scientific, 2011.

[3] D. Zhu, Y. Ait-Amirat, A. N'Diaye, and A. Djerdir, "On-line state of charge estimation of embedded metal hydride hydrogen storage tank based on state classification," *Journal of Energy Storage*, vol. 42, p. 102950, 2021.

[4] A. Cecilia, *Advances in Nonlinear Observer Design for State and Parameter Estimation in Energy Systems*. Springer Nature, 2023.

[5] T. Puleston, A. Cecilia, A. Clemente, R. Costa-Castelló, and M. Serra, "Kazantzis-kravaris/luenberger observer for the joint estimation of vanadium flow battery concentrations and side-reaction rates," *Journal of Energy Storage*, vol. 139, p. 118760, 2025.

[6] M. Chen, R. Costa-Castelló, C. Batlle, and J. Na, "Metal hydride storage tanks real-time state of charge estimation based on nonlinear observer with a non-observable subsystem," *Applied Energy*, vol. 399, p. 126448, 2025.

[7] M. Chen, A. Cecilia, J. Na, C. Batlle, and R. Costa-Castelló, "Metal hydride storage tank state of charge estimation: A switched observer approach," *IEEE Transactions on Control Systems Technology*, pp. 1–12, 2025.

[8] A. L. J. Keow, A. Mayhall, M. Cescon, and Z. Chen, "Active disturbance rejection control of metal hydride hydrogen storage," *International Journal of Hydrogen Energy*, vol. 46, no. 1, pp. 837–851, 2021.

[9] G. Besançon, *Nonlinear observers and applications*. Springer, 2007, vol. 363.

[10] P. Bernard, V. Andrieu, and D. Astolfi, "Observer design for continuous-time dynamical systems," *Annual Reviews in Control*, vol. 53, pp. 224–248, 2022.

[11] R. Hermann and A. Krener, "Nonlinear controllability and observability," *IEEE Transactions on Automatic Control*, vol. 22, no. 5, pp. 728–740, 1977.

[12] D. Astolfi and L. Praly, "Integral action in output feedback for multi-input multi-output nonlinear systems," *IEEE Transactions on Automatic Control*, vol. 62, no. 4, pp. 1559–1574, 2016.

[13] M. Chen, C. Batlle, B. Escachx, R. Costa-Castelló, and J. Na, "Multi-objective identification of a metal hydride tank lumped parameter model," *Journal of Energy Storage*, vol. 139, p. 118759, 2025.

[14] ——, "Sensitivity analysis and calibration for a two-dimensional state-space model of metal hydride storage tanks based on experimental data," *Journal of Energy Storage*, vol. 94, p. 112316, 2024.

[15] A. Isidori, *Lectures in feedback design for multivariable systems*. Springer, 2017.

[16] E. D. Sontag and Y. Wang, "On characterizations of the input-to-state stability property," *Systems & Control Letters*, vol. 24, no. 5, pp. 351–359, 1995.